Alberto Battistel*, Hegoa Craamer Lizarraga, Maite Termenon, and Knut Möller

Multifrequency bioimpedance device based on the Analog Discovery 2: performance and characterization

https://doi.org/10.1515/cdbme-2023-1134

Abstract: Bioimpedance spectroscopy can be used to investigate the composition and monitor the human body, organs, tissues, or cell cultures by measuring the voltage developed by the injection of small alternating currents at different frequencies. These currents are injected sequentially through a frequency sweep and a with a Howland current source or one of its modifications. However, the frequency sweep is not time efficient and introduces problems with data coherence in the case of bioinstability. On the other hand, the Howland current source requires high precision matching between its components. In this contribution we developed a custom-made device for bioimpedance measurements based on a multisine current waveform and on a negative-feedback topology for the current source. Measurements on passive elements showed that the device had less than $1\,\Omega$ and 0.05° uncertainty in the frequency range between $500\,\mathrm{Hz}$ and $200\,\mathrm{kHz}$ for impedance between $1\,\mathrm{k}\Omega$ and $10\,\mathrm{k}\Omega$. The measurements were affected by an inductive artifact connected with the limited common-mode rejection at high frequencies. Nevertheless, we could characterize the artifacts through a fitting procedure to recover the expected value of the targeted impedance.

Keywords: Bioimpedance, impedance spectroscopy, FPGA, Analog Discovery 2, multisine, broadband excitation, instrumentation amplifier, common-mode rejection, multifrequency, current source.

1 Introduction

In bioimpedance spectroscopy measurements, small alternating currents are injected in the human body, organ, tissue, or cell culture under investigation. From the generated voltage fluctuations the impedance of the sample is recovered. This provides a plethora of information in an easy and non-invasive fashion also without the usage of any ionizing radiation [1].

Examples of bioimpedance measuring applications range from clinical monitoring [2], impedance plethysmography [3], and wound healing [4] among others.

The safety of electrical measurements is regulated by the IEC 60601 standard which limits the admissible amplitude of the alternating current to the milliampere or sub-milliampere range depending on the frequency [5].

To comply with regulations precise and reliable current sources are employed. These are usually based on the Howland current source topology or one of its modifications [6]. However, these topologies require several elements to be matched to very high precision in order to guarantee an elevated output impedance.

Bioimpedance is usually measured through a frequencies sweep with each frequency measured sequentially one after the other [7]. This can give problems with data consistency because of bioinstability which is produced by the natural occurring movements of the subject, but also by the blood perfusion, respiration, or other physiological related mechanisms. Thus, there are potential variations in the impedance between the application of consecutive frequencies. These variation could invalidate the measurements. Therefore, additional mathematical tests based for example on Kramers-Kronig relations are necessary to ensure the data quality [8].

To overcome this problem broadband excitations are preferred. Furthermore, broadband excitations are also effective in terms of measuring time and injected energy [9]. Among broadband excitations, Kallel et al. pointed out that a multisine with logarithmically distributed frequencies has the highest spectrum amplitude and it is also one of the most energy-effective [10].

In this work we show a custom implementation and the performances of a device for bioimpedance spectroscopy based on a four-electrode setup and a multsine current waveform. The device was made of an analog front-end implementing a negative-feedback current source topology. This front-end was powered by an field-programmable gate array (FPGA) which provided the analog-to-digital and digital-to-analog converters necessary to produce and record the multisine.

***Corresponding author: Alberto Battistel,** Institute of Technical Medicine (ITeM), Furtwangen University, Jakob-Kienzle-Strasse 17, 78054 Villingen-Schwenningen, Germany, e-mail: alberto.battistel@hs-furtwangen.de
Hegoa Craamer Lizarraga, Maite Termenon, Biomedical Engineering Department, Faculty of Engineering, Mondragon Unibertsitatea (MU-ENG), Loramendi, 4; 20500 Mondragón, Spain.
Knut Möller, Institute of Technical Medicine (ITeM), Furtwangen University, 78054 Villingen-Schwenningen, Germany

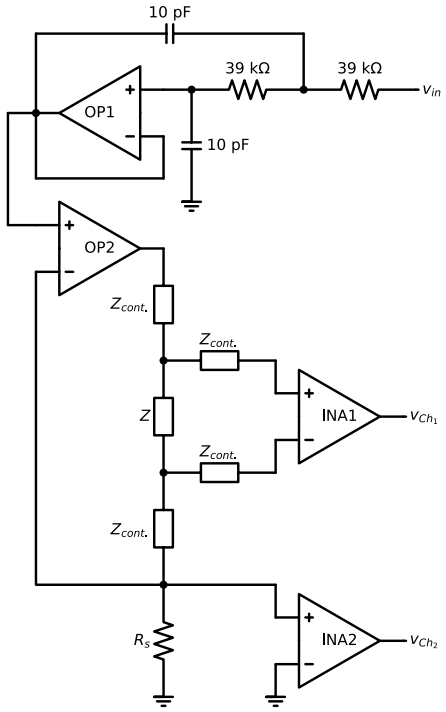

Fig. 1: Functional schematic of the custom bioimpedance device. Z represents the impedance to measure.

Besides, here we discuss some measurements artifacts and their relations with the limited bandwidth and common mode rejection of the operational amplifiers employed in the setup.

2 Analog Front-end Development

As shown in Figure 1 the analog front-end for the bioimpedance device employed two operational amplifiers (OP1-2) and two instrumentation amplifiers (INA1–2).

The signal coming at v_{in} first passed through a lowpass filter (OP1). This filter was implemented with Sallen–Key topology and had a cutoff frequency of circa $400\,\mathrm{kHz}$. Subsequently OP2 served as voltage-controlled current source. This opamp operated in a negative-feedback topology converting the filtered signal into the current i according to the size of R_s. For our tests R_s was set to $10\,\mathrm{k\Omega}$. This gave a peak-to-peak magnitude for the current of circa $200\,\mu\mathrm{A}$. This current magnitude was well-below the limits specified by the IEC 60601.

v_{in} was where the digital-to-analog converter of the FPGA was connected and the multisine excitation was fed into the system.

The two instrumentation amplifiers (INA1–2) recovered the voltage drop across the targeted impedance Z and the current across the resistor R_s, respectively. This voltage was directly proportional to the current i circulating into the system. The two INAs conditioned the signals to be send to the analog-to-digital converter of the FPGA at v_{Ch_1} and v_{Ch_2}.

The FPGA also provided the $\pm 5\,\mathrm{V}$ for the voltage rails which powered OP1–2 and INA1–2 (not shown).

The analog front-end was developed on a breadboard using an OP37E and an LMC6001 as OP1 and OP2, respectively, and two INA128P as INA1–2. The FPGA was the Analog Discover 2 from Digilent controlled using the python library `pydwf` [11]. A measurement consisted of setting up the multisine excitation for the waveform generator of the FPGA and synchronously acquiring the signals at at v_{Ch_1} and v_{Ch_2}.

3 Artifact Model and Fitting

The measurements were affected by the limited common mode rejection of the INA1 at high frequencies. Then the measured impedance Z_m could be modeled as:

$$Z_m = K(f)R_s + \frac{K(f)Z}{2} + Z \tag{1}$$

which was a function of the targeted impedance Z, the measuring resistor R_s, and a factor $K(f)$. The factor $K(f)$ was function dependent and represented the fact that a part of the voltage developed on R_s passed into v_{Ch_1} because of the insufficient common mode rejection. This rejection was up to $120\,\mathrm{dB}$ at low frequencies for an INA128P [12], but it deteriorated quickly at higher frequencies. Here $K(f)$ was successfully modeled as a high-pass filter:

$$K(f) = \frac{j2\pi f a_0}{j2\pi f + 2\pi f_0}. \tag{2}$$

It is easy to see that if the common mode rejection is perfect $K(f) = 0$ and $Z_m = Z$.

This model was implemented into a fitting which was performed minimizing the χ^2:

$$\chi^2 = \sum_i \frac{\mathrm{Re}(Z_i - Z_m)^2}{\mathrm{Re}(\sigma_i)^2} + \frac{\mathrm{Im}(Z_i - Z_m)^2}{\mathrm{Im}(\sigma_i)^2} \tag{3}$$

where i is the frequency index and σ_i are the experimental uncertainties recovered for example from repeated experiments. Note that separating the complex values into real and imaginary part as in eq. (3) was equivalent to consider them as independent experimental samples. This assumption was ensured by the uncorrelated noise distribution of the standard deviations.

The uncertainties σ_j for the parameters P_j to fit (Z, a_0, and f_0) were derived as in [8] with $\sigma_j^2 = C_{j,j}$, where $C =$

α^{-1} and α was defined from the partial derivatives of the fitted model Z_m versus the parameters P:

$$\alpha_{j,k} = \sum_i \frac{1}{\sigma_i^2} \left[\frac{\partial Z_m}{\partial P_j} \frac{\partial Z_m}{\partial P_k} \right] \tag{4}$$

The errors on the estimation of the fitted parameters P_j was then considered as twice σ_j.

4 Methods

The measurements were performed with a sampling frequency of 1 MHz. Typically, the multisine comprised 18 quasi-logarithmically distributed frequency between 500 Hz and 400 kHz. All the frequencies had the same amplitude and they were chosen avoiding common small integers multiples. Also they had a minimal bin spacing between harmonics as specified by Koster et al. [13].

The impedance was calculated post-acquisition through fast Fourier transforms (fft) employing a periodic Blackmann-Harris window function. The device performances were characterized employing several resistors as Z and $Z_{cont.}$.

5 Results

Figure 2 shows the experimental uncertainty obtained repeating the same measurement 100 times for a set of three resistor ranging between 10 kΩ and 100 Ω. For all three resistors both the standard deviation on the absolute value and the phase of the recorded impedances was plotted against the frequency.

The uncertainty on the absolute value was below 1 Ω until 200 kHz for all resistors and grew exponentially beyond that point (Figure 2 a). Particularly the variation was the lowest between 10 kHz and 100 kHz, with the values for 100 Ω reaching 0.2 Ω.

The phase uncertainty was below 0.05° for 1 kΩ and 10 kΩ until 300 kHz. The values for 100 Ω were consistently higher in all the frequency range. We attributed this to the low ohmic drop generated on the resistor, i.e. only 20 mV peak-to-peak in this case.

In Figure 3 the Nyquist plot for two resistors used as target impedance Z and their respective fitting, which were performed following the model (1), are displayed. The plot of a resistor should be a single point on the real axis at the value of the resistor: at 98.8 Ω and 1761 Ω for figure a) and b), respectively. Instead, at the highest frequencies the impedance displayed an inductive behavior and the magnitude of the imaginary part increased. This was a consistent behavior for all measurements and was attributed to the failing common mode rejection of INA1 at high frequencies.

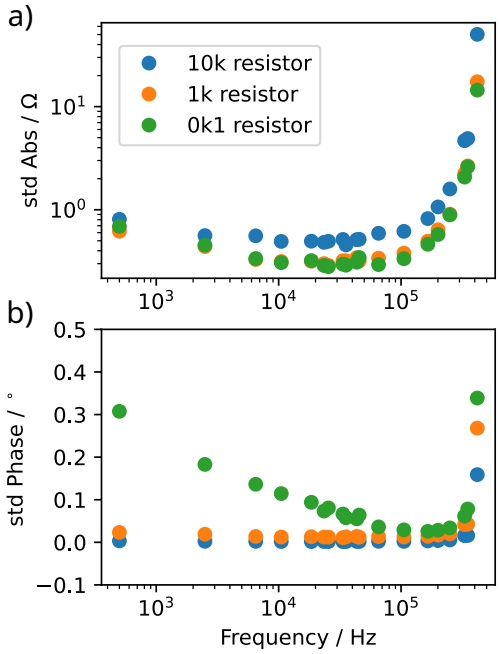

Fig. 2: Experimental uncertainties for three different resistor sizes (10 kΩ, 1 kΩ and 0.1 kΩ) and 100 measurements. a) standard deviation on the absolute value of the impedance. b) standard deviation on the phase.

For Figure 3 the estimated values of the Z, recovered with the model (1), were 99.47(15) Ω and 1760.96(23) Ω for figure a) and b), respectively. The values of a_0 and f_0 were 0.3541(31) and 8.029(71) × 10^5 Hz for a) and 0.826(10) and 1.270(15) × 10^6 Hz for b).

6 Discussion

Contrary to many works on bioimpedance, here the analog front-end employed a negative-feedback topology to realize a voltage-controlled current source. The advantage of this topology laid in its simplicity given that it was realized with a single operational amplifier and a single resistor. Also its output impedance was limited by the non-inverting gain. In fact, when the load impedance, which in Figure 1 would be given by $Z + 2Z_{cont.}$, was much larger than R_s the bandwidth of the device was lowered and smaller amplitude alternating currents could be injected at the highest frequencies. With this topology the best performances are theoretically achieved when the load impedance has a magnitude comparable to R_s. In this case the gain is two and the voltage-controlled current source has a bandwidth matching half the gain–bandwidth product of the operational amplifier (1.3 MHz for the LMC6001 [14]).

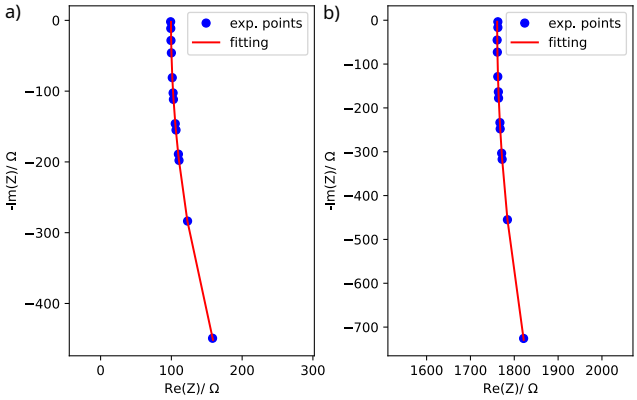

Fig. 3: Experimental measurements with fitting: a) $Z = 98.8\,\Omega$, b) $Z = 1761\,\Omega$.

On the other hand, the main disadvantage of this topology was that it consumed a large portion of the available voltage swing on the resistor R_s and it made impossible to adjust independently the resistor used to set and to measure the current amplitude.

Figure 2 shows that the measurement uncertainty did not have a strong dependency on the value of the target impedance. Also the uncertainties grew particularly large beyond $200\,\mathrm{kHz}$.

As visible from Figure 3 the measurement were affected by inductive artifacts. We attributed these artifacts to the insufficient common mode rejection of INA1 and we accounted for it in the fitting model. This model could well resolve and eliminate the artifact. In fact, the values recovered for the targeted impedances were in very good agreement with the experimental ones.

On the other hand, we observed that the values for a_0 and f_0 were not the same between measurements performed on different targeted impedances. This precluded the possibility to use fixed known values for them, as for example through a series of calibrations.

7 Conclusions

We successfully developed and characterized a custom device for bioimpedance measurements in four electrodes configuration. This device was capable of reliable measurements employing a broadband multisine and a negative-feedback VCCS with frequencies between $0.5\,\mathrm{kHz}$ and $200\,\mathrm{kHz}$.

Although an inductive artifact appeared it was easily removed by including it in a fitting model.

Author Statement

Research funding: This research was partially supported by Deutsche Forschungsgemeinschaft (DFG) project TAP (project number 498224366) and the project AIRLobe (32-7545.220/42/1). Conflict of interest: Authors state no conflict of interest.

References

[1] Grimnes S, Martinsen Ø G. Alpha-dispersion in human tissue. *J. Phys.: Conf. Ser.*, 2010. 224(1):012073.

[2] Dutt A G, Verling M, Karlen W. Wearable bioimpedance for continuous and context-aware clinical monitoring. In *2020 42nd Annual International Conference of the IEEE Engineering in Medicine & Biology Society (EMBC)*. 2020 pp. 3985–3988.

[3] Ferreira J, Seoane F, Lindecrantz K. Portable bioimpedance monitor evaluation for continuous impedance measurements. Towards wearable plethysmography applications. In *2013 35th Annual International Conference of the IEEE Engineering in Medicine and Biology Society (EMBC)*. 2013 pp. 559–562.

[4] Lukaski H C. Evolution of bioimpedance: A circuitous journey from estimation of physiological function to assessment of body composition and a return to clinical research. *Eur J Clin Nutr*, 2013. 67(1):S2.

[5] Naranjo-Hernández D, Reina-Tosina J, Min M. Fundamentals, Recent Advances, and Future Challenges in Bioimpedance Devices for Healthcare Applications. *Journal of Sensors*, 2019. 2019:1.

[6] Bertemes-Filho P, Vincence V C, Santos M M, Zanatta I X. Low power current sources for bioimpedance measurements: A comparison between Howland and OTA-based CMOS circuits. *Journal of Electrical Bioimpedance*, 2012. 3(1):66.

[7] Majzoub S, Allagui A, Elwakil A S. Time-Frequency Design of a Multi-Sine Excitation With Random Phase and Controllable Amplitude for (Bio) Impedance Measurements. *IEEE Access*, 2022. 10:31641.

[8] Orazem M E, Tribollet B. *Electrochemical Impedance Spectroscopy*. Wiley, Hoboken; N.J, 2008.

[9] Sanchez B, Vandersteen G, Bragos R, Schoukens J. Optimal multisine excitation design for broadband electrical impedance spectroscopy. *Meas. Sci. Technol.*, 2011. 22(11):115601.

[10] Kallel A Y, Bouchaala D, Kanoun O. Critical implementation issues of excitation signals for embedded wearable bioimpedance spectroscopy systems with limited resources. *Meas. Sci. Technol.*, 2021. 32(8):084011.

[11] Welcome to pydwf ! — pydwf 1.1.11 documentation. https://pydwf.readthedocs.io/en/latest/welcome.html#project-hosting.

[12] Instruments T. INA12x Precision, Low-Power Instrumentation Amplifiers, 2022.

[13] Koster D, Du G, Battistel A, La Mantia F. Dynamic impedance spectroscopy using dynamic multi-frequency analysis: A theoretical and experimental investigation. *Electrochim. Acta*, 2017. 246:553.

[14] Instruments T. LMC6001 Ultra,Ultra-Low Input Current Amplifier, 1995.